



**Fermi National Accelerator Laboratory**

**FERMILAB-Pub-89/213**

## **Demonstration of Electron Beam Self-Focusing in Plasma Wake-Fields \***

J. B. Rosenzweig

*Fermi National Accelerator Laboratory*

*P.O. Box 500*

*Batavia, Illinois 60510*

P. Schoessow, B. Cole, C. Ho, W. Gai, R. Konecny,  
S. Mtingwa, J. Norem, M. Rosing, and J. Simpson

*Argonne National Laboratory*

*Argonne, Illinois 60439*

October 16, 1989

\* Submitted to Physics of Fluids B, special issue of invited papers from the 1989 APS Division of Plasma Physics Annual Meeting, Anaheim, California, November 13-17, 1989.



October 16, 1989

# DEMONSTRATION OF ELECTRON BEAM SELF-FOCUSING IN PLASMA WAKE-FIELDS

J. B. ROSENZWEIG

*Fermi National Accelerator Laboratory*

*P.O. Box 500, M.S. 306,*

*Batavia, Illinois 60510*

P. SCHOESSOW, B. COLE,<sup>†</sup> C. HO, W. GAI, R. KONECNY,  
S. MTINGWA, J. NOREM, M. ROSING, AND J. SIMPSON

*High Energy Physics Division*

*Argonne National Laboratory*

*Argonne, Illinois 60439*

## ABSTRACT

In this paper, we report the direct observation of wake-field self-focusing of an electron beam in plasma. The dynamics of beam self-pinching and the fast collisionless evolution of a Bennett-like, near-equilibrium profile are examined theoretically and computationally. The experimental results are compared to predictions of the analysis, and discussed in the context of application to the plasma lens and the plasma wake-field accelerator.

Submitted to *Physics of Fluids B*, special issue of invited papers from the 1989 APS Division of Plasma Physics Annual Meeting, November 13-17, 1989.

<sup>†</sup>Present address: SSC Laboratory, Dallas, Texas 75237.

## 1. Introduction

In the Plasma Wake-field Accelerator,<sup>[1-4]</sup> (PWFA) charged particles are accelerated in the potentially ultra-high gradient fields supported by plasma waves driven in the wake of an intense particle beam. These wake-fields can also be strongly focusing,<sup>[4]</sup> and this fact has led to the proposal of employing plasma wake-fields to create a powerful final focusing lens for use in a future linear  $e^+e^-$  collider.<sup>[5-9]</sup> This device has been termed a plasma lens, and can generate greater than MG/cm focusing gradients for typical linear collider parameters. In the course of the initial experimental investigations into the physical mechanisms of the PWFA at Argonne National Laboratory,<sup>[10,11]</sup> evidence for very strong self-focusing of the intense driving electron beam was accumulated. Relevant observations included improved transmission of the driving beam through the final limiting aperture of the plasma source when plasma was present, larger beam divergence of the driving beam as measured at the spectrometer focal plane downstream of the plasma, and deflection of a secondary lower energy, low intensity ‘witness’ beam by the driver’s transverse wake-fields in the plasma. In addition, the measurement of the accelerating wake-fields yielded convincing indirect evidence of beam self-focusing, as at higher driving beam currents the wake-fields were enhanced in both amplitude and in nonlinearity beyond what was expected assuming the driving beam did not pinch. The degree of nonlinearity in the wake-fields provided an estimate on the self-pinched driving beam radius; this estimate agreed well with what is calculated from the theory of plasma focusing.<sup>[11]</sup>

Previous observations made during the PWFA experiments at Argonne thus constitute an indirect case for the existence of plasma wake-field focusing and support for some of the predictions of the relevant theory. This is not a satisfactory state of affairs, however, as the theoretical estimates of the observed degree of wake-field wave nonlinearity were based on a rough synthesis of three-dimensional linear<sup>[5]</sup> and one-dimensional nonlinear<sup>[12-14]</sup> PWFA theories, which in total add up to a convincing plausibility argument. In order to make the expla-

nation of the observed phenomena in these experiments complete it is necessary to measure the actual self-pinched beam profiles in the plasma. In addition, the large volume of theoretical work done on plasma lenses to date, in which researchers have attempted to reliably predict the behavior of these devices as focusing elements, demands experimental validation. With these factors as motivation, a set of measurements of the self-pinched beam profiles in plasma have been undertaken. The results of these measurements are reported in this paper.

It is necessary to provide in some detail the theoretical background for understanding the processes involved in electron beam self-focusing in a plasma. The discussion naturally breaks down into two distinct subjects, the plasma wake-field response to the beam, and the subsequent dynamics of the beam as it is influenced by these wake-fields. A review of previous work on the plasma response is presented below, which is necessary for examining the effects of the beam profile and the plasma density on the form and strength of the focusing wake-fields. As in a certain limit these wake-fields become nearly independent of the plasma density and depend only on the beam profile, the self-consistent evolution of the beam is treated next. Analytical models of the self-pinch process are employed; laminar flow is assumed in calculating the initial focusing dynamics, and the Maxwell-Vlasov equation is utilized to discuss the asymptotic approach to self-pinched Bennett equilibrium. Computer simulations are shown to complement and clarify the conclusions of the analysis. After the theoretical context is established, the results of the experimental measurements are presented and compared with the theory. The conclusions of the previous experiments are then re-examined in light of this new data.

## 2. Linear Plasma Wake-field Theory

The two-dimensional linear theory of plasma wake-fields, as formulated by P. Chen,<sup>[6]</sup> provides a simple model for calculating expected focusing wake-fields in the presently relevant experimental regime. This theoretical treatment, which is described below, applies to a cold plasma with density perturbation small compared to the unperturbed electron density, and assumes an unchanging beam density profile. From the cold plasma fluid equations with the ions assumed stationary, a linearized equation can be derived which describes small amplitude plasma electron response driven by a relativistic electron beam. The equation can be written as

$$\frac{\partial^2 n_1}{\partial \xi^2} + k_p^2 n_1 = -k_p^2 n_b, \quad (2.1)$$

where  $n_1 = n - n_0$  is the deviation of the plasma electron density from equilibrium density  $n_0$ ,  $k_p \equiv 2\pi/\lambda_p = \omega_p/c = \sqrt{4\pi r_e n_0}$  is the plasma wave number, and  $n_b$  is the beam density. The linearization of the equations requires that  $n_1 \ll n_0$ .

If one assumes that the beam density distribution can be expressed in separable form as  $n_b = \rho_b h(r)g(\xi)$ , where  $\rho_b$  is the maximum beam density,  $r$  is the radial coordinate, and  $\xi = z - ct$  is the longitudinal coordinate measured from the center of the bunch, the solution of Eq. (2.1) is given by<sup>[6]</sup>

$$n_1 = -k_p \rho_b h(r) \int_{\xi}^{\infty} g(\xi') \sin(k_p(\xi' - \xi)) d\xi' \equiv -\rho_b h(r) G(k_p \xi). \quad (2.2)$$

Note that the plasma charge density  $-en_1$  has the same transverse dependence as the beam density  $h(r)$ . The longitudinal response, however, is described by  $G(k_p \xi)$ , a convolution integral over the beam density ahead of the point in question with the causal Green's function solution to Eq. (2.1). If the beam is short compared with the plasma wavelength, then the convolution integral is large behind the beam and negligible inside of the beam. This corresponds physically to the impulse excitation of a large amplitude plasma wave in the beam's wake with

very little plasma motion occurring inside the beam, which is desirable for plasma wake-field acceleration. If the beam is not short compared to a plasma wavelength then the amplitude of the excited wave is smaller, as the plasma electrons have time to react to and partially neutralize the beam space charge density. In the limit that the longitudinal beam profile is smoothly varying and is long compared to a plasma wavelength, then  $G(k_p \xi) \simeq -g(\xi)$ , which implies  $n_1 \simeq -n_b$ . The beam can be nearly space charge neutralized, and very small amplitude plasma waves are driven in the beam's wake. The beams employed in the present experiments have approximately cylindrically symmetric bi-Gaussian distributions, and we can write our initial beam density as  $n_b = \rho_b \exp(-r^2/2\sigma_r^2 - \xi^2/2\sigma_z^2)$ . If the beam is long, one expects  $n_1$  to also be bi-Gaussian, with small oscillations at the plasma frequency superimposed on this equilibrium configuration. It can be seen from Eq. (2.2) that the amplitude of these oscillations is approximately  $\rho_b \exp[(-k_p \sigma_z)^2/2]$ , and thus vanish exponentially in the long beam limit.

Once one knows the plasma response, the wake-fields can be found directly<sup>[4]</sup> or through solution of the wake potential equations.<sup>[5]</sup> It is not necessary for present purposes to examine these solutions in detail, as in the regime of interest the calculation of the wake-fields simplifies considerably. If the beam is narrow compared to a plasma wavelength ( $k_p \sigma_r \ll 1$ ), a condition which is approximately satisfied in the experiments, then the plasma return current, which is localized within a disk of radius of  $k_p^{-1}$ , flows mainly outside of the beam and the beam current density is not locally neutralized. Thus in a long, narrow beam satisfying  $k_p \sigma_r \ll 1 \ll k_p \sigma_z$  the beam is charge, but not current neutralized, and the wake-fields reduce to the magnetic self-focusing forces of the beam. As the beam is relativistic, these fields can be calculated trivially by using Gauss' law. For the cylindrically symmetric case, the transverse wake-fields in this limit are given by

$$W_r = -4\pi e^2 \rho_b g(\xi) \left[ \frac{1}{r} \int_0^r h(r') dr' \right]. \quad (2.3)$$

For non-uniform profiles this expression does not yield linear focusing as in the

case of a perfect lens. This effect gives rise to serious aberrations, one of the limitations of the plasma lens. The subject of aberrations and their effect on plasma lens performance has been examined extensively in the literature.<sup>[6] [7] [9]</sup>

### 3. Beam Dynamics: Initial Self-Pinch

Much of the previous work on plasma lenses concerns the effect of a thin plasma lens on the transverse profile of a particle beam. In the present experiments, however, the plasma column is long compared to the focal length of the lens, and the beam dynamics are much more complex. In Ref. 6, there is a treatment of the problem of the thick lens correction to the thin lens which includes the effects of finite beam emittance and the raising of the focusing strength as the beam becomes more dense inside the lens (cf. Eq. (2.3)). This analysis is not strictly applicable to the present case, and therefore a simpler approximation is chosen, that of laminar flow of the beam particles. Since the transverse wakefields felt by a particle depend only on the enclosed current, which is conserved in laminar flow, and on the radius of the particle, each particle obeys an equation of motion for paraxial trajectories derivable from a logarithmic potential,

$$r'' + \frac{C(r_0)}{r} = 0, \quad (3.1)$$

where ' indicates a derivative with respect to distance of propagation  $z$ , and  $C(r_0)$  is a constant dependent on initial radius  $r_0$ . Near the center of a cylindrical Gaussian this constant is given by  $C(r_0) \simeq (\nu/\gamma)(r_0/\sigma_r)^2$ , where  $\gamma$  is the Lorentz factor and we have introduced the Budker parameter  $\nu$ , which is the number of particles per unit length measured in classical electron radii  $r_e$ . Integrating Eq. (3.1), the distance from the plasma boundary to the first focus is calculated,

$$s = \frac{1}{\sqrt{2C(r_0)}} \int_0^{r_0} \frac{dr}{\sqrt{\log(r_0/r)}} = r_0 \sqrt{\frac{\pi}{2C(r_0)}}. \quad (3.2)$$

For a Gaussian initial profile one has  $s \simeq \sigma_r \sqrt{\pi\gamma/\nu}$ . In these experiments the number of particles per bunch is  $N = 3.2 \times 10^{10}$ , the rms bunch length  $\sigma_z = 2.1$

mm and  $\gamma = 42$ , so the Budker parameter is  $\nu = 1.6 \times 10^{-2}$ . The beam is thus expected to come to its initial focus  $s \simeq 8$  cm, which is well before the end of the plasma column of length  $L = 35$  cm.

It is difficult to analytically estimate the minimum pinched beam radius in the presence of aberrations and finite initial emittance, because the transverse profile of the beam changes so dramatically as it focuses under the influence of nonlinear fields. This subject can be addressed most straightforwardly by use of computer simulations. Computational treatments using a particle-in-cell code of this and related aspects of the self-pinching process will be presented below. Before proceeding to the computational work, an analytical model of the beam's approach to equilibrium is explored.

#### 4. Beam Dynamics: Approach to Equilibrium

The transverse phase space dynamics of the beam under the influence of its self-focusing magnetic fields can be calculated in principle from the Maxwell-Vlasov equations, the self-consistent combination of the Maxwell electromagnetic field equations and the Vlasov equation, which is written

$$\frac{\partial f}{\partial t} + (\gamma m_e)^{-1} \mathbf{p}_\perp \cdot \nabla_{\mathbf{r}_\perp} f + \mathbf{F} \cdot \nabla_{\mathbf{p}_\perp} f = 0. \quad (4.1)$$

Here  $f(\mathbf{r}_\perp, \mathbf{p}_\perp)$  is the beam's transverse distribution function and  $\mathbf{F}$  is the Lorentz force arising from the charge and current distribution under consideration. In this case the force is due to the transverse wake-fields given by Eq. (2.3), which depend on the distribution of the beam particles in configuration space.

At this point it can be remarked that, because of the large nonlinearities in the radial focusing force and the effects of the individual particles' angular momentum, all particles have different effective betatron wave-numbers describing the periodicity of their orbits. Thus the initial coherent self-focusing motion of a set of particles decoheres as the particles become out of phase with each

other, and the situation is approached where the distribution in configuration space becomes uncorrelated with the distribution in momentum space, *i.e.* the distribution seeks an equilibrium through collisionless or Landau damping. This approach to equilibrium through phase decoherence in the particle oscillations, whereby the coherent radial beam motion dissipates, was in fact initially sketched out by Bennett in 1955, who termed the effect ‘mixing’.<sup>[15]</sup> This effect is similar to a phenomenon, also referred to as decoherence, observed in the experimental study of nonlinear transverse dynamics in synchrotrons.<sup>[16]</sup>

As a specific type of stationary distribution is of present interest, the Maxwell-Vlasov equation is now written in cylindrically symmetric equilibrium as

$$\frac{p_r}{\gamma m} \frac{\partial f}{\partial r} + W_r \frac{\partial f}{\partial p_r} = 0, \quad (4.2)$$

and the distribution function is assumed separable in coordinate and momentum dependence,  $f(r, p_r) = R(r)P(p_r)$ , because of the decorrelating effects of the nonlinearities. This assumption will be validated later by our computer simulations.

Upon substitution of the radial dependence of the magnetic self-force  $W_r$  from Eq. (2.3), and separation of variables, one obtains the momentum equation

$$\frac{\partial P}{\partial p_r} = -\frac{\alpha p_r}{\gamma m} P, \quad (4.3)$$

where  $-\alpha$  is the separation constant, and the radial equation

$$\frac{\partial R}{\partial r} = -R \frac{2\alpha e^2 \beta^2}{r} \int_0^r R(r') r' dr'. \quad (4.4)$$

The solution to the Eq. (4.3) is, of course, a Gaussian (thermal) distribution,

$$P = \sqrt{\frac{\alpha}{2\pi\gamma m}} \exp[-\alpha p_r^2 / 2\gamma m]. \quad (4.5)$$

The solution to the radial equation corresponding to this thermal equilibrium in

momentum space is a Bennett profile<sup>[16]</sup> which has the form

$$R(r) \sim n(r) = \frac{\rho_b}{[1 + (r/a)^2]^2} \quad , \quad (4.6)$$

where  $a$  is the Bennett radius. The usual expression for the Bennett radius relates it to the beam Debye length  $\lambda_D$ , with  $\beta \simeq 1$ ,

$$a^2 = 8\lambda_D^2 = \frac{2kT_\perp}{\pi e^2 \rho_b} = \frac{2kT_\perp}{\nu m c^2} a^2 \quad , \quad (4.7)$$

which only specifies the relationship between the beam transverse temperature and current, not the radius, which cancels out of the equation. This uncertainty can be removed by invoking an approximate constraint on the asymptotic form of the distribution function.

To derive this constraint, note that from the form of the self-fields of a cylindrically symmetric beam and the associated Maxwell-Vlasov equation that the phase space density must be constant at  $(\mathbf{r}_\perp, \mathbf{p}_\perp) = (\mathbf{0}, \mathbf{0})$ , as from Eq. (4.1) we see that  $\partial f / \partial t = 0$  there. If one takes an original four-dimensional phase space density corresponding to a cylindrically symmetric bi-Gaussian profile, and equates its initial value of  $f(\mathbf{0}, \mathbf{0})$  to the final value of  $f(\mathbf{0}, \mathbf{0})$  associated with the Bennett equilibrium, the Bennett radius is given by

$$a^2 = \frac{4\epsilon_n^2}{\gamma\nu} \quad , \quad (4.8)$$

where  $\epsilon_n = \beta\gamma\epsilon$  is the initial normalized emittance.

This argument is not strictly rigorous, however. Even though  $f(\mathbf{0}, \mathbf{0})$  is a constant of the motion, the form of the asymptotic state that we have assumed is not completely correct. It has been known for some time that the Bennett profile, being a state in thermal equilibrium, can evolve from a different initial state due to the thermalizing influence of multiple scattering of beam particles off the background plasma ions.<sup>[17]</sup> The distribution function can become smooth

during this collisional process and thus approach the equilibrium solution to the Maxwell-Vlasov equation, which is the product of two smooth functions, a Bennett radial profile and Gaussian momentum profile.

In the case of the collisionless damping, however, the near-equilibrium state evolves from the initial pinch by filamentation of the beam phase space as it spirals under the influence of its own nonlinear self-fields. This filamentation process does not greatly affect the center of the distribution in phase space if the self-focusing forces there are nearly linear, which is the case for conditions not too far from equilibrium. This is because near equilibrium the small amplitude orbits in phase space are well behaved rotations about the fixed point of simple harmonic motion,  $(0,0)$ . On the other hand, large amplitude orbits experience very nonlinear fields, and the filamentation is quite pronounced in these regions of phase space. Since the derivation given above of the asymptotic Bennett radius is concerned with the final values of  $f(\mathbf{r}_\perp, \mathbf{p}_\perp)$  at or near  $(0,0)$ , the fact that the motion near this point is well behaved makes the argument, which depends critically on approximation of the distribution as a smooth function at small amplitudes, quite accurate for cases relatively close to equilibrium.

If the motion is not well behaved even for small amplitude particles, as happens if the initial conditions are too far from equilibrium (e.g.  $a \ll \sigma_r$ ), then the distribution function filaments near the origin in phase space, and the approximation of the actual distribution function as a product of smooth continuous functions is not as good. Filamentation at small amplitudes thus causes the asymptotic Bennett radius to be larger, and we rewrite Eq. (4.8) as an inequality,  $a \geq 2\epsilon_n/\sqrt{\gamma\nu}$ . In fact, other effects, such as a deviation from the assumed initial cylindrical symmetry, spurious plasma oscillations or nontrivial return current density inside the beam radius will serve to strengthen this inequality. All of these effects are present in experiments to some extent.

In the limit of applicable beam-plasma parameters,  $k_p\sigma_z \gg 1 \gg k_p\sigma_r$ , some predictions can be made concerning the outcome of experiments. In the present

experiments the normalized emittance  $\epsilon_n = 3 \times 10^{-4}$  rad-m. Since the maximum in the beam current at  $\xi = 0$  corresponds to a maximum Budker parameter of  $\nu_0 = 1.6 \times 10^{-2}$ , the minimum Bennett radius predicted from the Vlasov analysis is  $a_0 \geq 0.72$  mm. This pinching is not uniform along the length of the beam, as in the model it depends on the current at a given point in  $\xi$ , a fact that can be reflected by writing  $\nu(\xi) = \nu_0 \exp(-\xi^2/2\sigma_z^2)$ . One then has  $a(\xi)^{-2} = a_0^{-2} \exp(-\xi/2\sigma_z^2)$ , and the equilibrium density profile on axis is proportional to  $\exp(-\xi/\sigma_z^2)$ , *i.e.* the bunch is effectively shortened on axis by a factor of  $\sqrt{2}$ .

## 5. Beam Dynamics: Simulation

In order to examine the deviations from the approximate theoretical treatments presented to this point, particle-in-cell simulations of the beam motion have been performed. In these calculations, which employed a modified version of the code EMMA,<sup>[18]</sup> written by Noble to calculate the related problem of emittance growth in a space-charge dominated transport channel, cylindrical symmetry is assumed, longitudinal effects are ignored, and the wake-fields are calculated simply by using Eq. (2.3). The evolution of the beam distribution at one point in  $\xi$  can be quickly followed under these assumptions. Some relevant aspects of these computational results are presented here, which clarify the analytical work and provide more concrete predictions for the experimental data. These results are specialized in that the spurious effects of plasma oscillations are ignored in order to concentrate on the beam dynamics; fully electromagnetic  $2\frac{1}{2}$ -dimensional particle-in-cell simulations of beam self-focusing by plasma wake-fields have been performed previously.<sup>[9][19]</sup>

To begin, we examine the evolution of the peak beam density  $\rho_b/\rho_{b0}$  as it self-pinches, which is shown in Fig. 1. The longitudinal distances are given in units of  $k_\beta^{-1}$ , where  $k_\beta = \sqrt{\nu/\gamma\sigma_r^2}$  is the initial small amplitude betatron wavenumber in the beam's self-focusing wake-field. All parameters in the computations shown correspond to the strongest focusing experimental case, in which  $a/\sigma_r = 0.51$ ,

where the initial beam distribution function is Gaussian in momentum and coordinate and the beam is at a waist. The initial pinching occurs in  $k_\beta s = 1.27$ , which is in excellent agreement with the value of  $k_\beta s = \sqrt{\pi/2} \simeq 1.25$  derived in Eq. (3.2). The peak beam density is approximately 20 times the initial peak density at this point; after slight defocusing, it subsequently does not reach such large densities, but tends rapidly towards equilibrium. The maximum predicted equilibrium density associated with  $a/\sigma_r = 0.51$  is  $\rho_b/\rho_{b0} = 2(\sigma_r/a)^2 = 7.85$ . It appears that the equilibrium which develops is slightly less dense than this.

The fluctuations in the peak density have nearly damped after  $k_\beta z = 3$ , or one beam envelope oscillation, which is extremely quick. The degree to which the distribution function comes into equilibrium, *i.e.* approaches a separable Bennett-coordinate/Gaussian-momentum form, can be quantified by examining the correlation parameter  $\langle rr' \rangle / \epsilon_r$ . Here  $\epsilon_r = \sqrt{\langle r^2 \rangle \langle (r')^2 \rangle - \langle rr' \rangle^2}$  is the radial rms emittance. The evolution of this parameter is shown in Fig. 2. After initial large excursions associated with the first focus and defocus, the correlations then damp more slowly while oscillating with period  $k_\beta \lambda \simeq 4$ . These oscillations do not in large part reflect oscillation of the core of the beam, as these would have a period  $k_\beta \lambda = 2\pi(a/\sigma_r) \simeq 3.2$ , and would show up also in Fig. 1. The correlations are instead due to the spiralling ‘arms’ of the distribution, which occur at large amplitude and thus have a lower average wave-number. These spirals, which come into equilibrium more slowly than the beam core due to the decrease in focusing strength with amplitude and the larger initially empty regions of phase space with which they must mix, have been observed in the simulations; they are not shown in the interests of brevity. These results support the conclusion that the phase space correlations in the beam core indeed dissipate quickly, after one radial oscillation, as is necessary to apply the results of the analysis above.

It is apparent from Fig. 1 that the maximum beam density has stabilized by  $k_\beta z = 5$ , which corresponds to the length of the plasma column in these experiments. It is reassuring to plot the transverse profile of the beam density at this point, as is shown in Fig. 3, along with the Bennett profile from the

theoretical prediction of the Vlasov treatment. The calculated profile is slightly less dense and has a marginally wider core than the minimum-radius Bennett profile, indicating small effects due to phase space filamentation.

Thus the simulations confirm the major conclusions of the analytical approaches that have been developed, and give additional insight into the expected experimental results. The observation of core equilibration within  $k_{\beta}z = 3$  allows use of the results of the Vlasov treatment to predict the self-pinch beam radius, as this equilibration length is shorter than the plasma column in the measurements, which are now described.

## 6. Measurement of Self-focused Beam Profiles in Plasma

Experimental measurement of the self-focused beam profiles at the end of a 35 cm long, variable density hollow cathode arc plasma column<sup>[10]</sup> has been performed in the same laboratory as previous PWFA investigations, the Argonne Advanced Accelerator Test Facility<sup>[20]</sup> (AATF). As no secondary beam had to be created for the purpose of probing the wake-fields directly, the full intensity driving beam was passed through the AATF into the experimental region occupied by the plasma source. To restate, the beam pulse delivered to the plasma source has the following parameters;  $N \simeq 3.2 \times 10^{10}$  electrons, rms length  $\sigma_z \simeq 2.1$  mm transverse emittance  $\epsilon \simeq 7\pi$  mm-mrad, and  $\sigma_r \simeq 1.4$  mm. This experiment used the video data acquisition and analysis capabilities of the AATF, as well the one-picosecond resolution streak camera.

The streak camera is the basis of a diagnostic that allows measurement of the transverse profile of the beam as a function of longitudinal position in the beam. Physically, this scheme entails placing an opaque thin walled (to minimize multiple scattering effects) Cerenkov cell inside the anode, in direct contact with the downstream end of the plasma column. The design of this cell is heavily constrained by the difficulty of survival of this relatively fragile device in such a hostile environment as inside of an arc electrode. The wall in contact with the

plasma is  $450\text{ }\mu\text{m}$  (.005 radiation lengths) of aluminum at its narrowest region, a horizontal slit on which the beam is vertically centered. The beam profile at this horizontal slit is converted to a photon profile by Cerenkov radiation due to the beam electrons' interaction with 2 mm of xenon gas at atmospheric pressure. The beam electrons and Cerenkov photons exit the cell through a synthetic quartz window. The photon profile is then transported through a telescopic optics system and focused onto the horizontal slit of the streak camera, giving a swept image that reflects the transverse profile of the beam in the horizontal direction versus time in vertical (streak) direction. The resolution of the profile obtained is  $12\text{ }\mu\text{m}$  in the transverse dimension and 1 psec in time.

The time-resolved pictures of the self-pinch transverse beam profile reveal a great deal about both the plasma and beam dynamics involved in the beam self-focusing. We show in Fig. 4 contour plots of the streak camera picture of the spatially resolved beam intensity, where the vertical axis is time and the horizontal axis is the transverse (radial) dimension. The plot in Fig. 4(b) is the profile with no plasma, and the plot in Fig. 4(a) shows the self-pinch profile in the case where the plasma density  $n_0 = 6.0 \times 10^{13}\text{ cm}^{-3}$ . In terms of the initial beam profile, this corresponds to a beam length in plasma radians  $k_p \sigma_z \simeq 3$ , and is thus in the regime where the plasma space charge neutralizes the beam and magnetic self-focusing occurs. The dependence of the focusing strength on enclosed current density is apparent from the contour shapes. With no plasma present, the iso-intensity contours are approximately elliptical, as expected for a beam with Gaussian profiles in both longitudinal and transverse dimensions. The self-pinch profile, however, shows a transverse distribution which narrows noticeably towards the longitudinal midplane. The self-pinch longitudinal profile measured near the propagation axis is also steepened and effectively shortened in time. This phenomenon, which is explored in more detail below, is also apparent from inspection of the contours near the transverse beam center, as they also narrow noticeably near the current maximum.

The plots in Fig. 5 shows the transverse cross-section (a projection of the

most intense 0.5 mm long transverse strip) of both the cases from Fig. 4. In the case of no plasma present shown in Fig. 5(b), we also show a best fit of the data, to a Gaussian of width  $\sigma_r = 1.4$  mm, with a dashed line. With dense plasma present the self-pinched profile shown in Fig. 5(a) is obtained, with a best fit of the data, to a Bennett profile of radius  $a = 0.91$  mm, indicated by the dashed line. The agreement in form is about as good as would be expected on the basis of the profile shown in Fig. 3. Recall that the minimum predicted Bennett radius for this case is  $a_0 = 0.72$  mm. The experimentally measured value is larger by about 25% due to the effects previously mentioned; the beam does not have perfect cylindrical symmetry initially, and deviations from this ideal undoubtedly allow more filamentation and effective dilution of the phase space density of the beam. In addition, there are effects due to the plasma response; even in the high plasma density case considered here the product  $k_p \sigma_z$  which results on axis after pinching (due to the effective pulse shortening described above) is about 2.2, which is just on the border of the adiabatic regime of the plasma electron fluid motion where one can assume approximate charge neutralization of the beam. The focusing in the core of the beam can be lowered by the response lag of the plasma electrons to the larger gradients in the beam charge density.

The effects of varying the plasma density have been explored, and these phenomena are illustrated in Figs. 6 and 7. The width (FWHM) of the beam intensity profiles, obtained from projection of the most intense 0.5 mm long transverse strip of the beam image, plotted as a function of the plasma density are shown in Fig. 6. The pinched beam profiles are not as narrow as the plasma density is lowered past the condition that the the beam is long compared to a plasma wavelength. The focusing forces do not depend on the enclosed current, but on the current ahead of the point in question by a phase difference of  $\Delta k_p \xi \simeq \pi/2$ . Thus the most intense portion of the beam's focusing is dependent on the less intense leading edge, and is therefore not focused as strongly, as can be seen from Fig. 6. At low enough plasma density ( $n_0 < 10^{13} \text{ cm}^{-3}$ , or  $k_p \sigma_z < 1.2$ ), the focusing wake-fields are small inside of the beam, and large only behind

the beam, resulting in the nearly complete degradation of the observed focusing in Fig. 6. In intermediate cases, the maximum in the beam intensity on-axis occurs after the current maximum. This is displayed in Fig. 7, which shows the on-axis density profile obtained from projection of the most intense 0.2 mm wide longitudinal strip of the beam image, plotted for four plasma densities,  $n_0 = 0.9, 1.5, 2.9$  and  $6.0 \times 10^{13} \text{ cm}^{-3}$ , using dashed, dotted, dot-dashed and solid lines, respectively. The peak in density moves back as predicted, by an amount slightly less than  $\Delta k_p \xi = \pi/2$ . This is because the current, which the on-axis density is proportional to, falls towards the back of the beam. For low plasma densities this tends to lengthen the on-axis beam profile, but if  $k_p \sigma_z \gg 1$ , or equivalently  $k_p \sigma_z \gg \Delta k_p \xi$ , the on-axis profile is effectively shortened, as predicted by the above analysis of the asymptotic equilibrium profile. For the most dense case in Fig. 7,  $k_p \sigma_z = 3.25$ , and the rms length of the on-axis density profile is 1.6 mm, in good agreement with the naive prediction given above of  $2.1/\sqrt{2} = 1.5$  mm.

The final parametric dependence examined was the effect on the focusing of varying the number of particles in the beam. The beam intensity was lowered without changing the upstream optics by use of partially transmitting screens in the beam-line upstream of the AATF. In Fig. 8 the width (FWHM) of the beam profiles, obtained from projection of the most intense 0.5 mm long transverse strip of the beam image, is plotted as a function of the number of particles  $N$  in the beam, while holding the plasma density at  $n_0 = 2.9 \times 10^{13} \text{ cm}^{-3}$ . The beam width decreases with increasing beam intensity, which is anticipated from the theory, as the focusing strength is dependent on  $N^{1/2}$ .

## 7. Conclusions

In these experiments, the self-pinched state of a beam in a plasma has been observed. From theoretical and computational analysis, a model has been developed of how this state develops through fast collisionless damping of the beam's coherent motion. This damping is predicted to occur due to nonlinear focusing fields, after the beam has undergone an initial strong, coherent self-focus, and subsequent near-equilibration inside the plasma column. The experimental results are in qualitative agreement with the analytical and computational models. Deviations from behavior predicted by the model which can be attributed to effects of oscillatory plasma electron response have been explored experimentally. These observed effects are explained adequately by the linear theory of plasma wake-fields.

These experimental results have validated conclusions drawn from the nonlinear PWFA experiments,<sup>[11]</sup> in that the unexpectedly high degree nonlinearity was attributed to two now directly observed effects of plasma wake-field focusing – enhancement of the peak density, and the effective shortening of the beam profile on-axis. In addition, the present experiments further strengthen empirical support for the theoretical models used in plasma lens calculations. These investigations concerned plasma focusing and equilibration of the self-pinched beam. Plasma lenses are more likely to be of interest in or near the thin lens limit, however. The physical processes of beam focusing in this limit, while less intricate and difficult to predict than in the regime presently considered, still await direct experimental investigation. In addition, even though the beams have been observed to become much denser inside the plasma, the plasma response is still not too far from linear, as  $n_b < n_0$ . An alternative, and in some ways more attractive regime of plasma wake-field focusing is termed the underdense plasma lens.<sup>[8][9]</sup> In this scheme the beam is dense compared to the plasma, and the physics of the plasma response is qualitatively different. Demonstration of plasma focusing in this regime is planned for future experiments.

## ACKNOWLEDGEMENTS

One of the authors (JBR) acknowledges helpful discussions with R. Noble, J. Palkovic, L. Michelotti and E.P. Lee. This work supported by the U.S. Dept. of Energy, Division of High Energy Physics, Contract W-31-109-ENG-38.

## REFERENCES

1. P. Chen, J. M. Dawson, R. W. Huff, and T. Katsouleas, *Phys. Rev. Lett.*, **54**, 693 (1985).
2. T. Katsouleas, *Phys. Rev. A* **33** (1986) 2056.
3. R. D. Ruth, A. Chao, P. L. Morton, and P. B. Wilson, *Particle Accelerators* **17** (1985) 171.
4. R. Keinigs and M. Jones, *Physics of Fluids* **30**, 252 (1987).
5. P. Chen, *Particle Accelerators* **20** (1985) 171.
6. J. B. Rosenzweig and P. Chen, *Phys. Rev. D* **39**, 2039 (1989).
7. J. B. Rosenzweig, B. Cole, D. B. Cline, and D. J. Larson, *Particle Accelerators*, **24**, 11 (1988).
8. P. Chen, S. Rajagoplan, and J. B. Rosenzweig, *Phys. Rev. D* **40**, 923 (1989).
9. J.J. Su, T. Katsouleas, J. Dawson and R. Fedeles, UCLA Report PPG-1177, 1988 (unpublished).
10. J. B. Rosenzweig, D. B. Cline, B. Cole, H. Figueroa, W. Gai, R. Konecny, J. Norem, P. Schoessow, and J. Simpson, *Phys. Rev. Lett.* **61**, 98 (1988).
11. J. B. Rosenzweig, P. Schoessow, B. Cole, W. Gai, R. Konecny, J. Norem and J. Simpson, *Phys. Rev. A - Rapid Comm.*, **39**, 1586 (1989).
12. J. B. Rosenzweig, *Phys. Rev. Letters*, **58** (1987) 555, J. B. Rosenzweig, *Phys. Rev. A*, **38**, 3634 (1988).
13. T. Katsouleas and W. B. Mori, *Phys. Rev. Lett.*, **61**, 90 (1988).
14. A.Ts. Amatuni, S.S. Sekhpossian and E.V. Elbakian, Yerevan Preprint YerPhi-935(86)-86 Yerevan, USSR (1986).
15. W. H. Bennett, *Phys. Rev.* **45**, 890 (1934), and *Phys. Rev.* **98**, 1584 (1955).

16. A. Chao, D. Johnson, S. Peggs, J. Peterson, C. Saltmarsh, L. Sachinger, R. Meller, R. Siemann, R. Talman, D. Edwards, D. Finley, R. Gerig, N. Gelfand, M. Harrison, R. Johnson, N. Merminga, and M. Syphers, *Phys. Rev. Lett.* **61**, 2752 (1988).
17. E.P. Lee, *Phys. Fluids* **19**, 60 (1976).
18. R. J. Noble, to be published in *Proceedings of the 1989 Particle Accelerator Conference*, AIP 1989.
19. J.J. Su, T. Katsouleas, J. Dawson, P. Chen, M. Jones and R. Keinigs, *IEEE Trans. Plasma Sci.* **PS-15**,192 (1987).
20. H. Figueroa, W. Gai, R. Konecny, J. Norem, P. Schoessow, and J. Simpson, *Phys. Rev. Lett.* **60**, 2144 (1988).

## FIGURE CAPTIONS

- Figure 1. Peak calculated beam density  $\rho_b/\rho_{b0}$  as a function of  $k_\beta z$ , for initial condition  $a/\sigma_r = 0.51$ . For minimum equilibrium Bennett radius  $\rho_b/\rho_{b0} = 7.85$ .
- Figure 2. Calculated correlation parameter  $\langle rr' \rangle / \epsilon_r$  as a function of  $k_\beta z$ , for initial condition  $a/\sigma_r = 0.51$ .
- Figure 3. Histogram of the calculated beam density at  $k_\beta z = 5$  (the end of the plasma column in the experiments), for initial condition  $a/\sigma_r = 0.51$ . Solid line is the Bennett profile predict by the Vlasov treatment.
- Figure 4. Contour plots of the spatially resolved beam intensity, with x being the transverse (radial) coordinate and y the longitudinal (time) coordinate. (a) Beam density contour with plasma of density  $n_e = 6.0 \times 10^{13} \text{ cm}^{-3}$  present. (b) No plasma present.
- Figure 5. Plots of the transverse intensity profiles (a projection of the most intense 0.5 mm long transverse strip) of the contours in from Fig. 4. (a) With dense plasma present - the self-pinch profile (solid line) with a best fit

of the data to a Bennett profile of radius  $a = 0.91$  mm (dashed line). (b) With no plasma – the unpinched profile (solid line) with a best fit of the data to a Gaussian profile of width  $\sigma_r = 1.4$  mm (dashed line).

Figure 6. Width (FWHM) of the intensity profiles obtained from projection of the most intense 0.5 mm long transverse strip of the beam image, plotted as a function of the plasma density.

Figure 7. Longitudinal on-axis beam density profile obtained from projection of the most intense 0.2 mm wide longitudinal strip of the beam image, plotted for four plasma densities,  $n_0 = 0.9, 1.5, 2.9$  and  $6.0 \times 10^{13} \text{ cm}^{-3}$  (dashed, dotted, dot-dashed and solid lines, respectively).

Figure 8. Width (FWHM) of the intensity profiles obtained from projection of the most intense 0.5 mm long transverse strip of the beam, plotted as a function of the number of particles  $N$  in the beam ( $n_0 = 2.9 \times 10^{13} \text{ cm}^{-3}$  ).

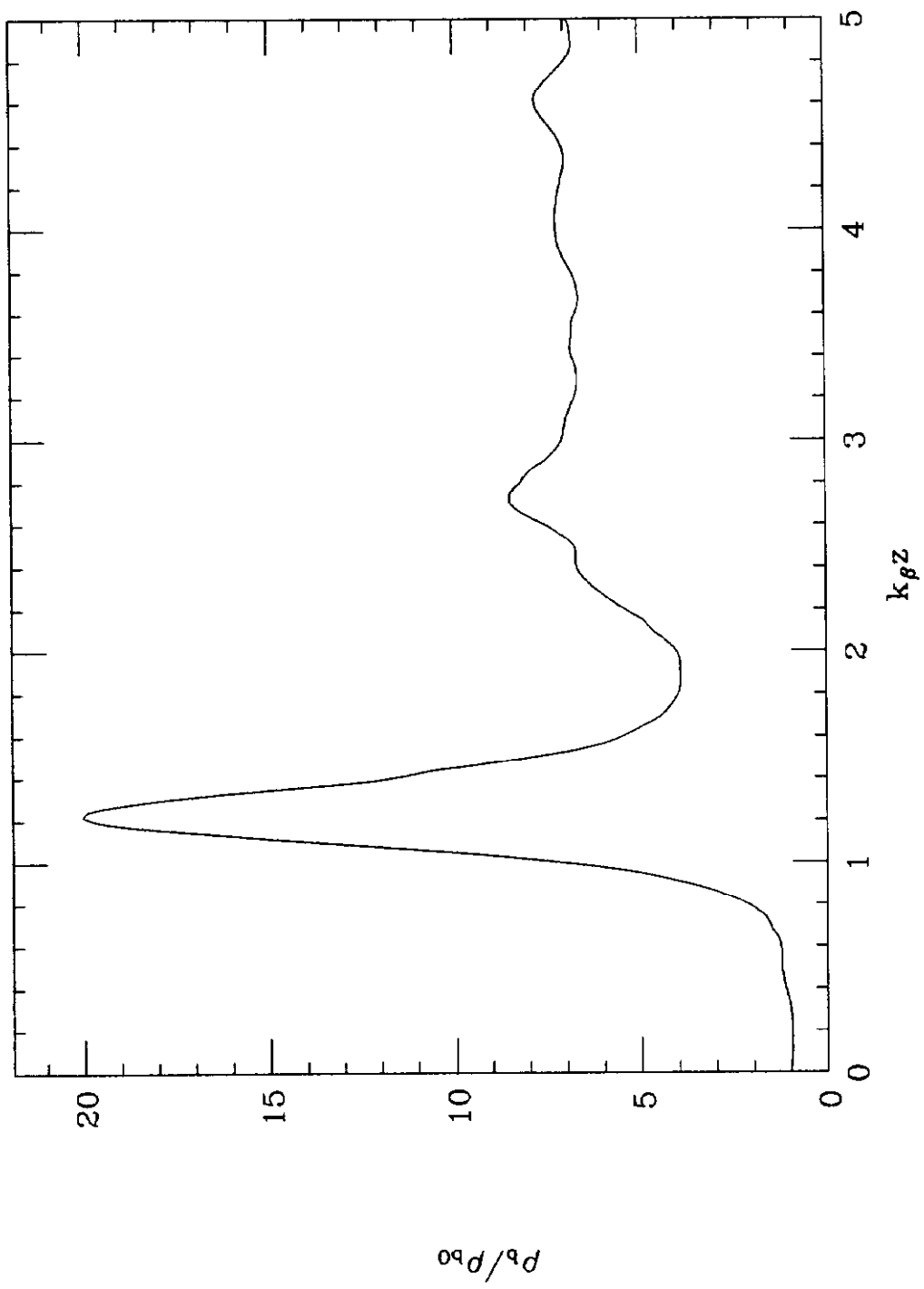


Figure 1

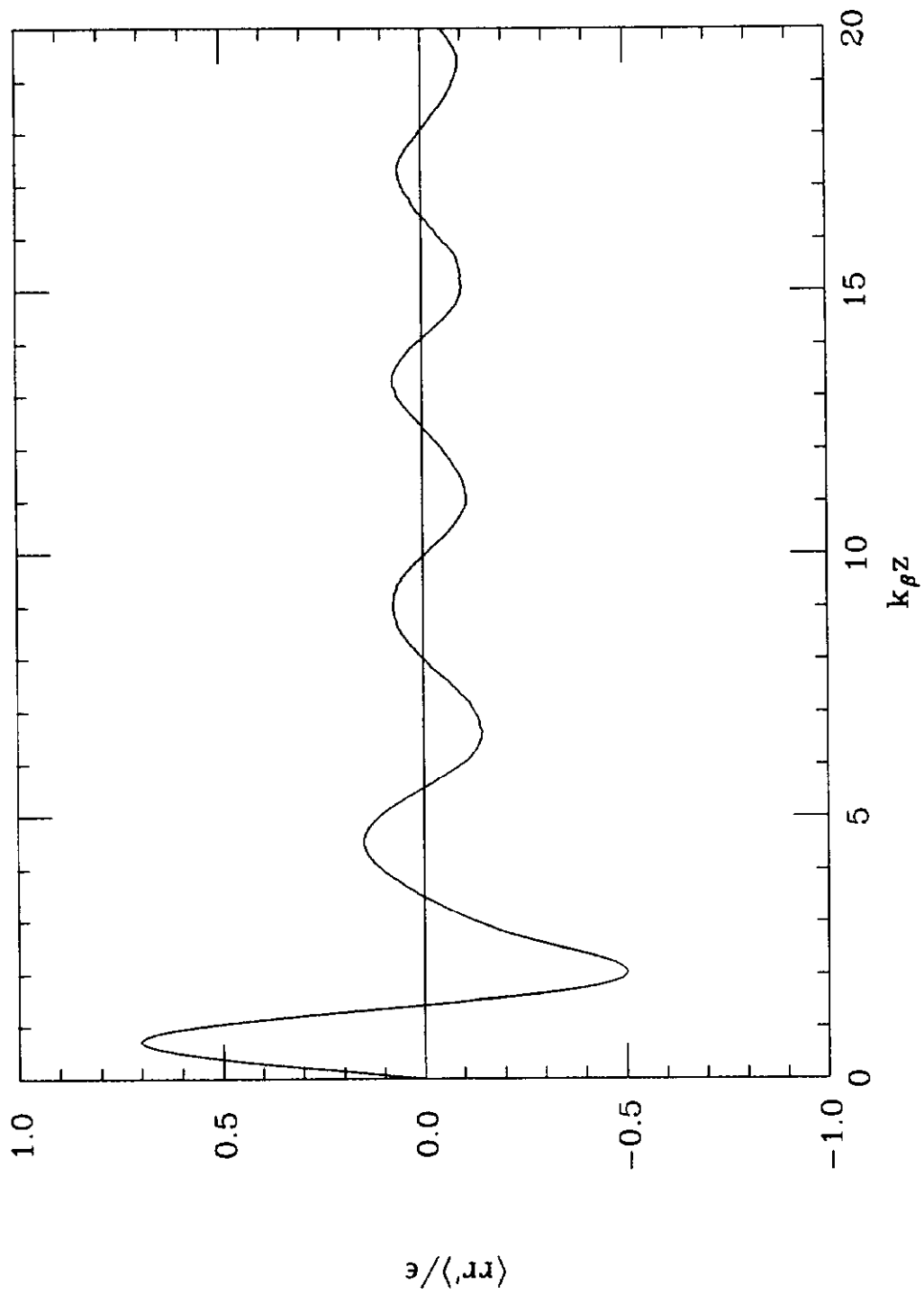


Figure 2

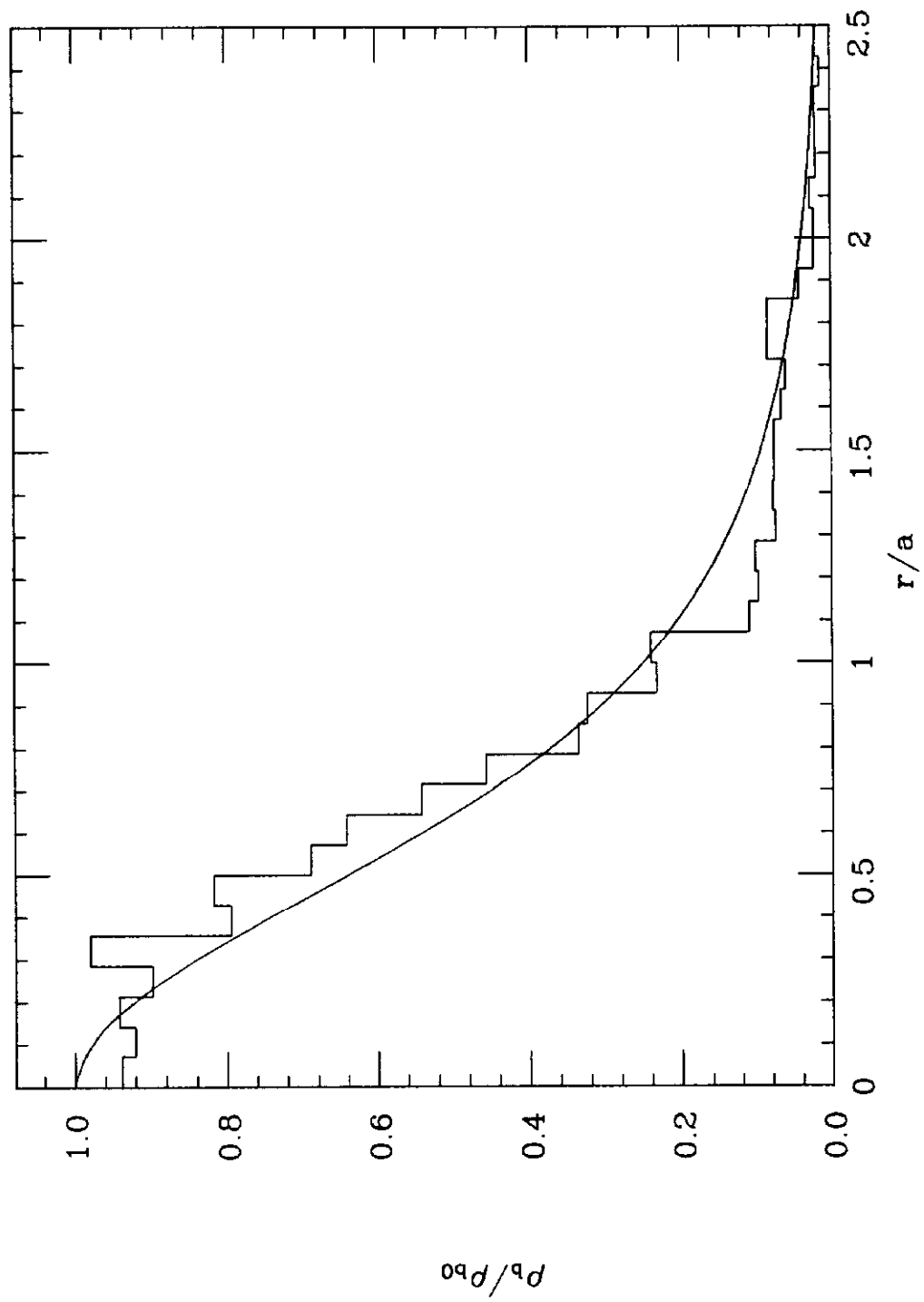


Figure 3

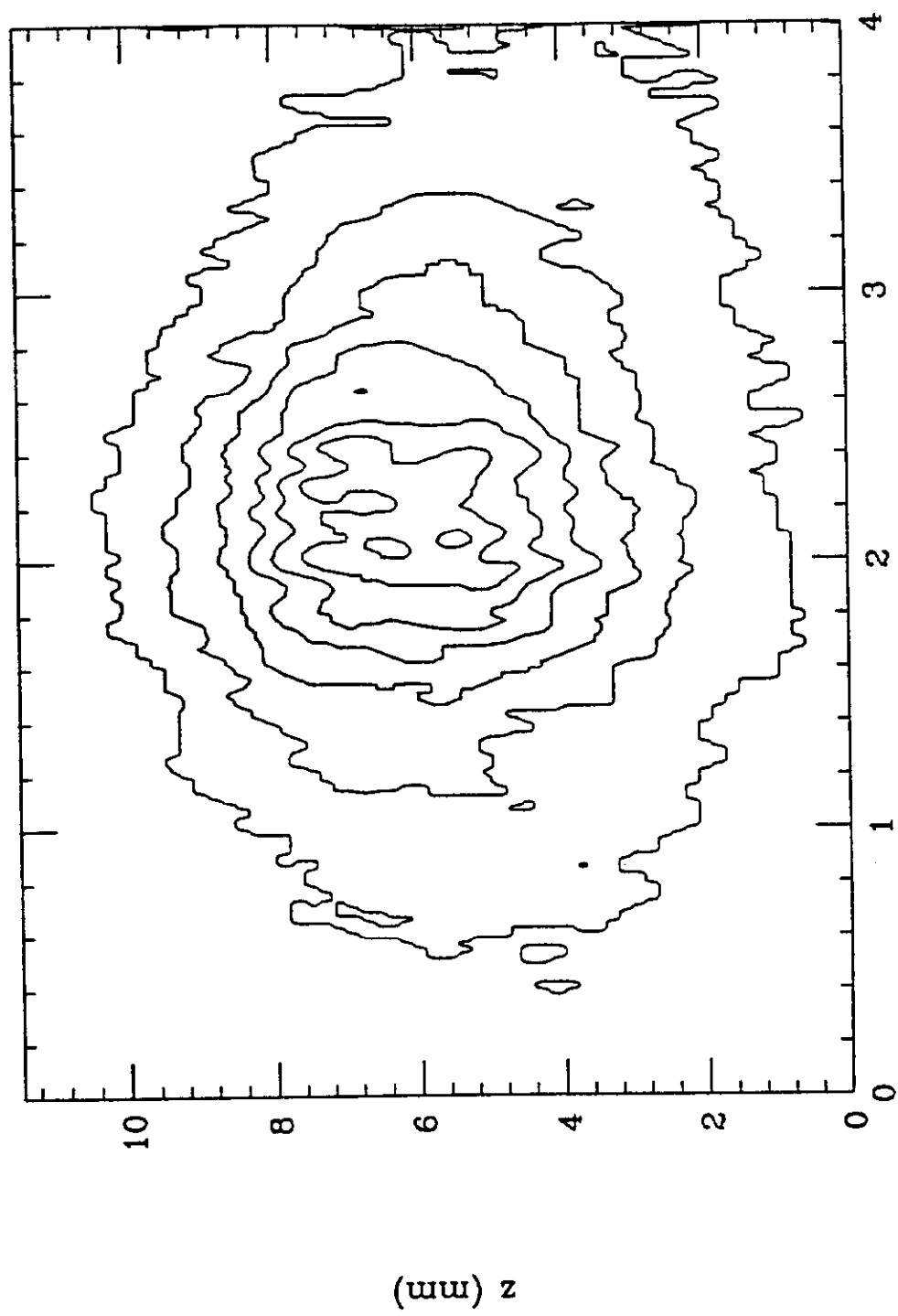


Figure 4(a)

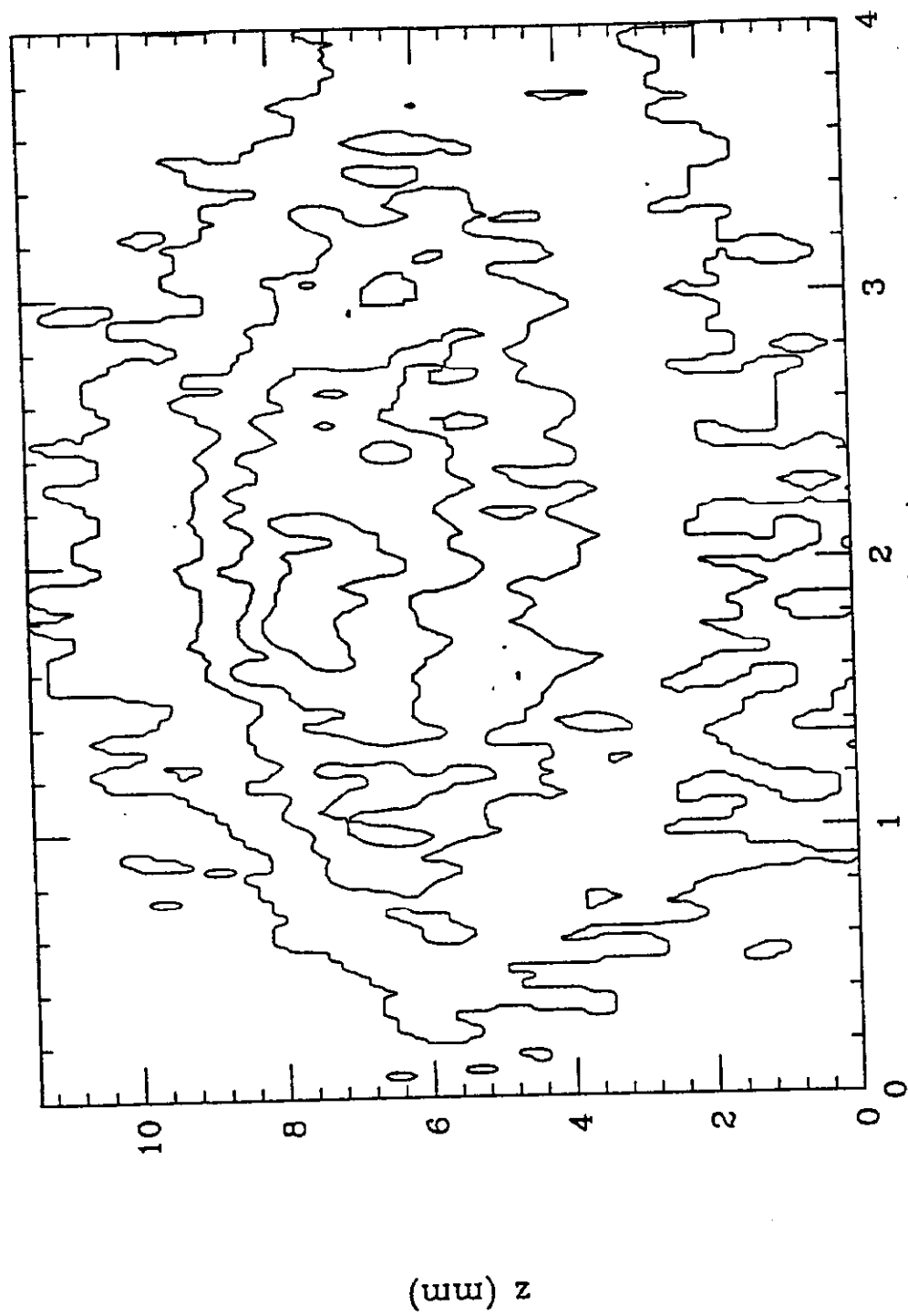


Figure 4(b)

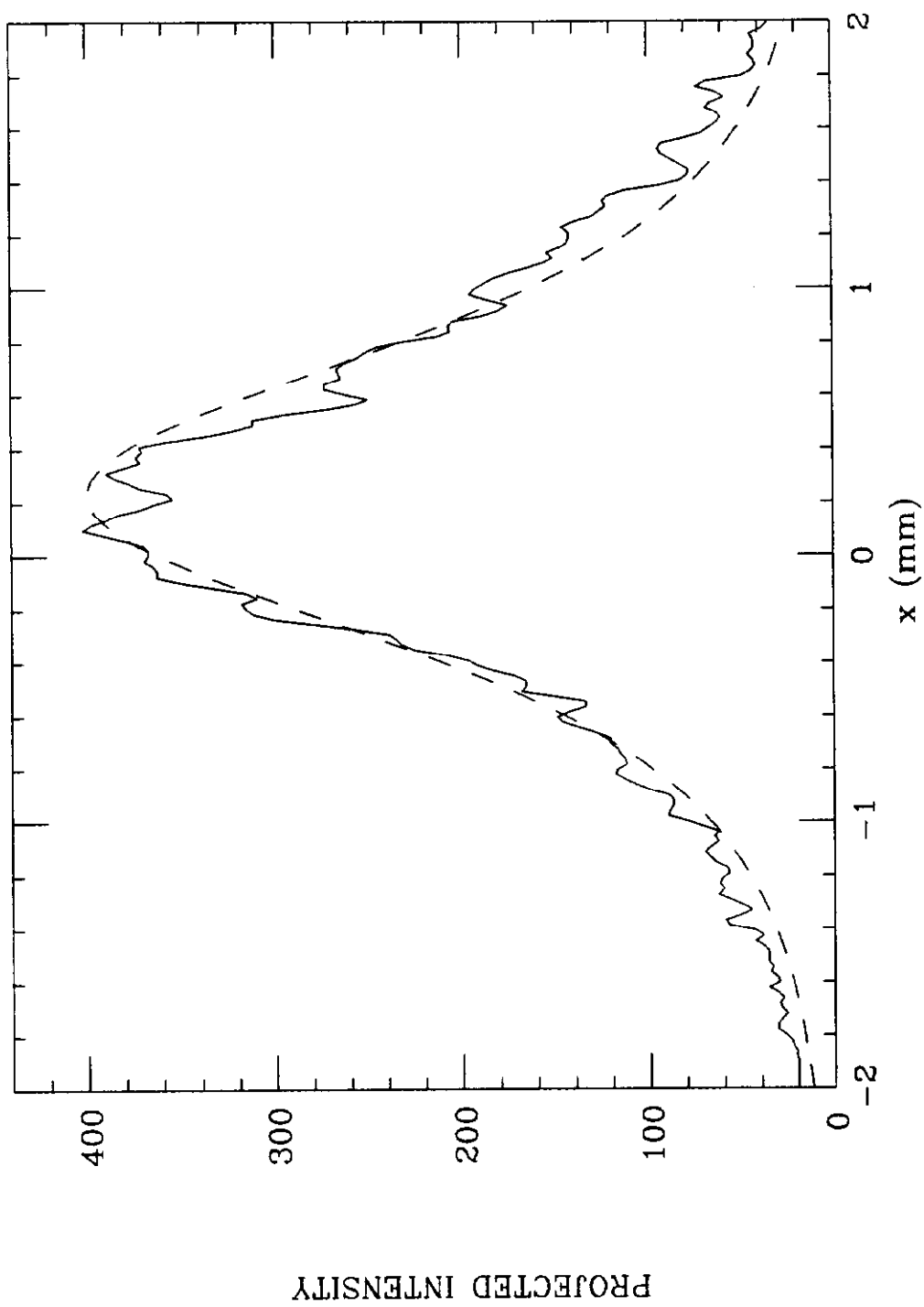


Figure 5(a)

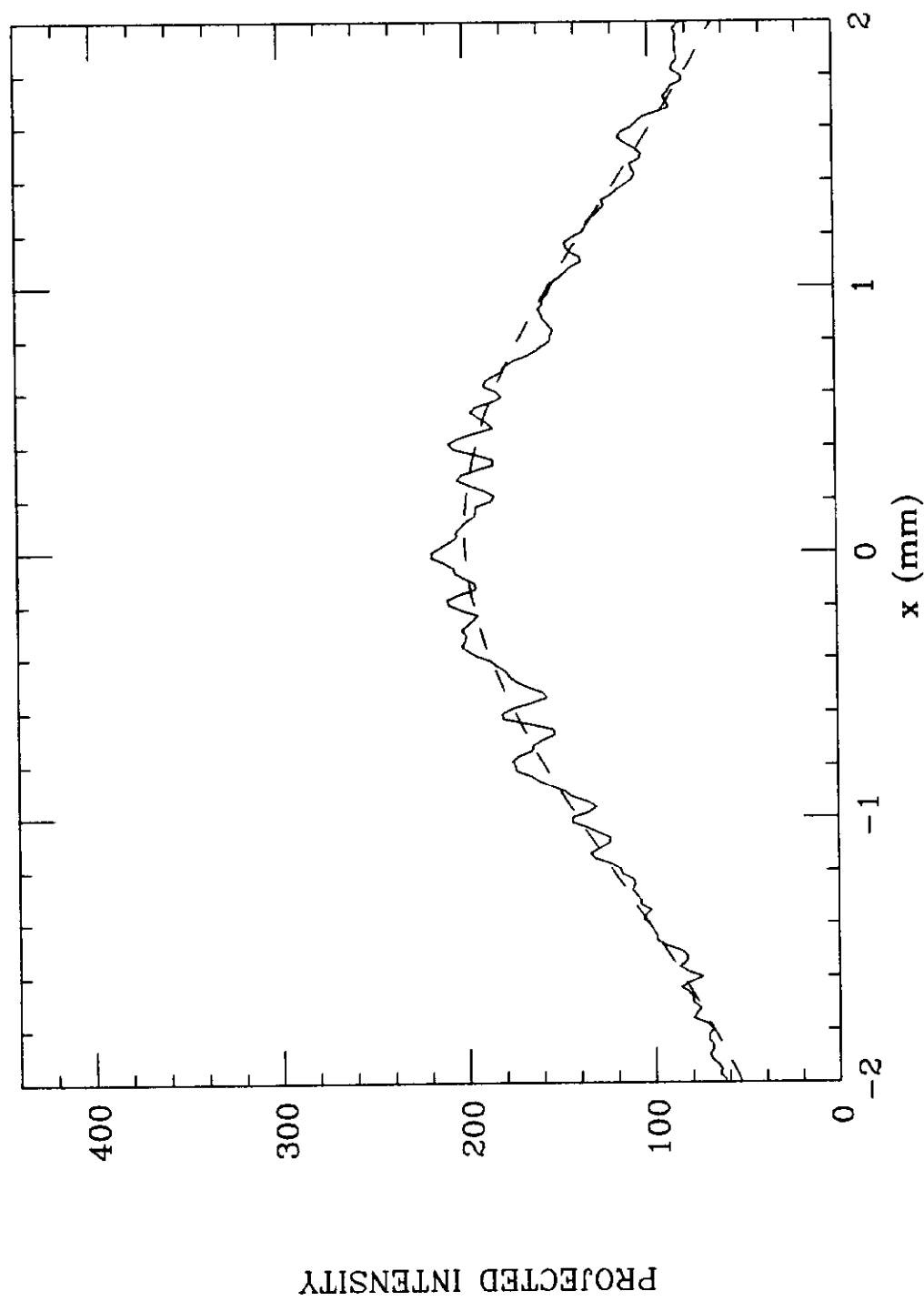


Figure 5(b)

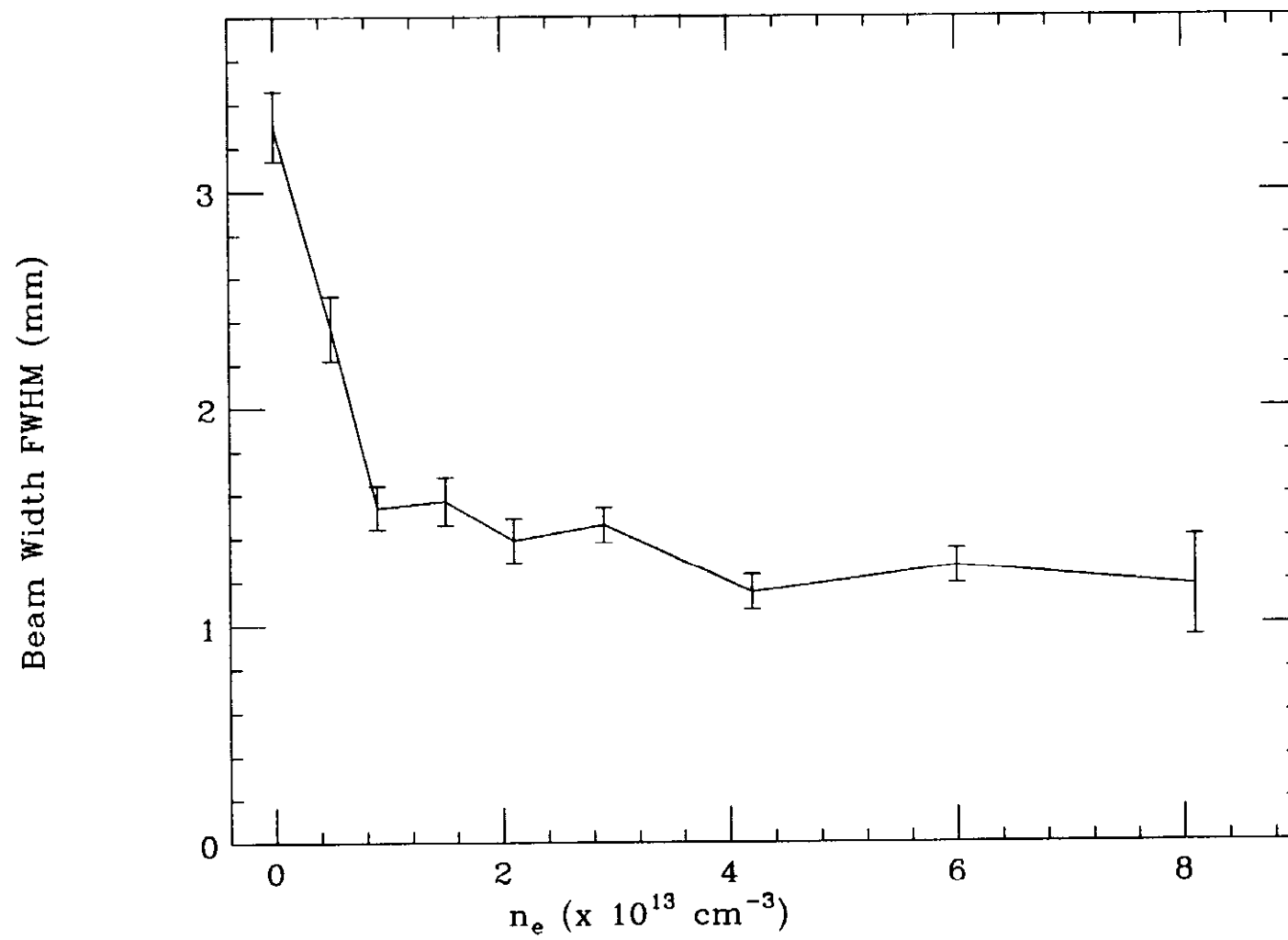


Figure 6

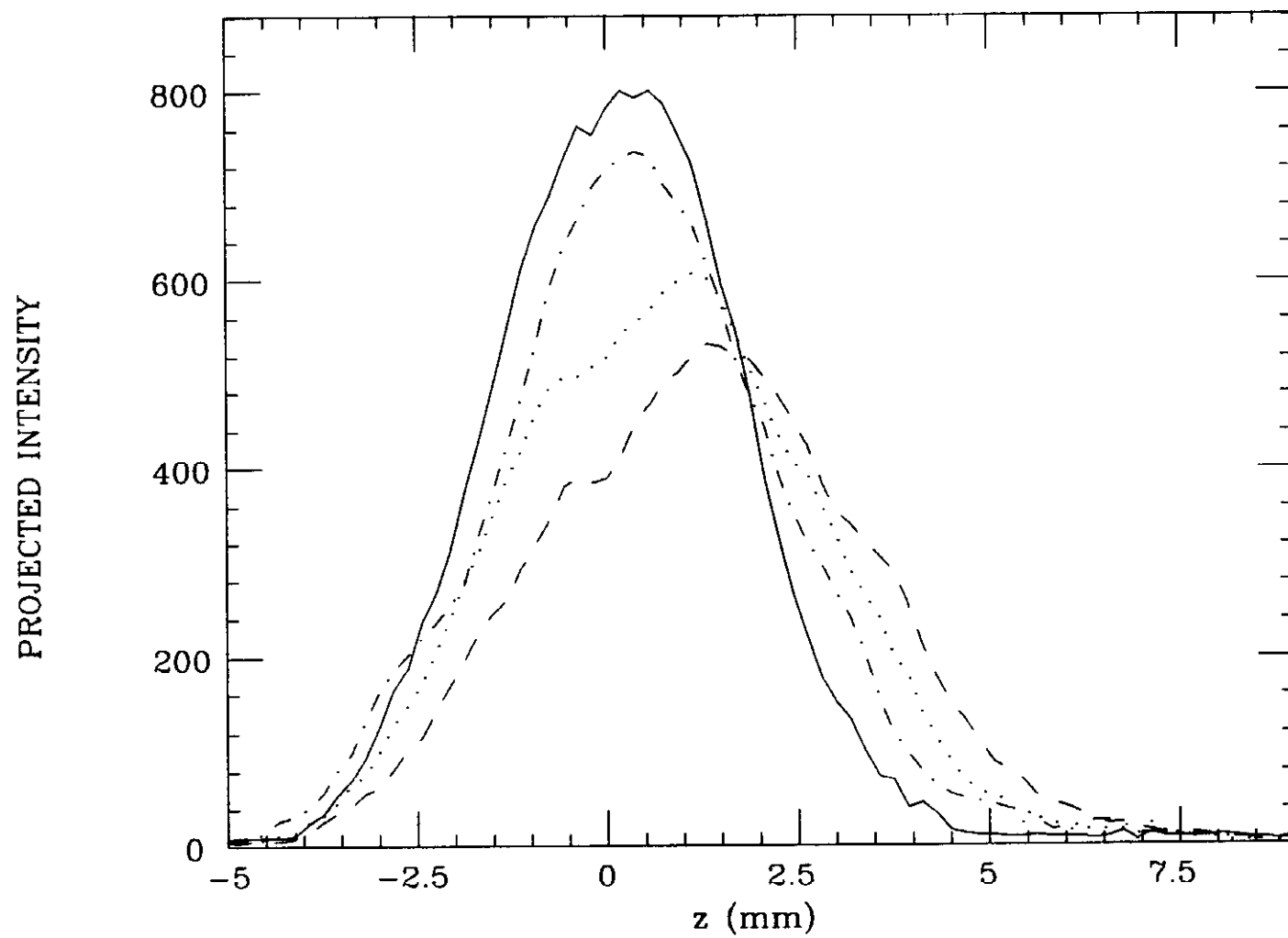


Figure 7

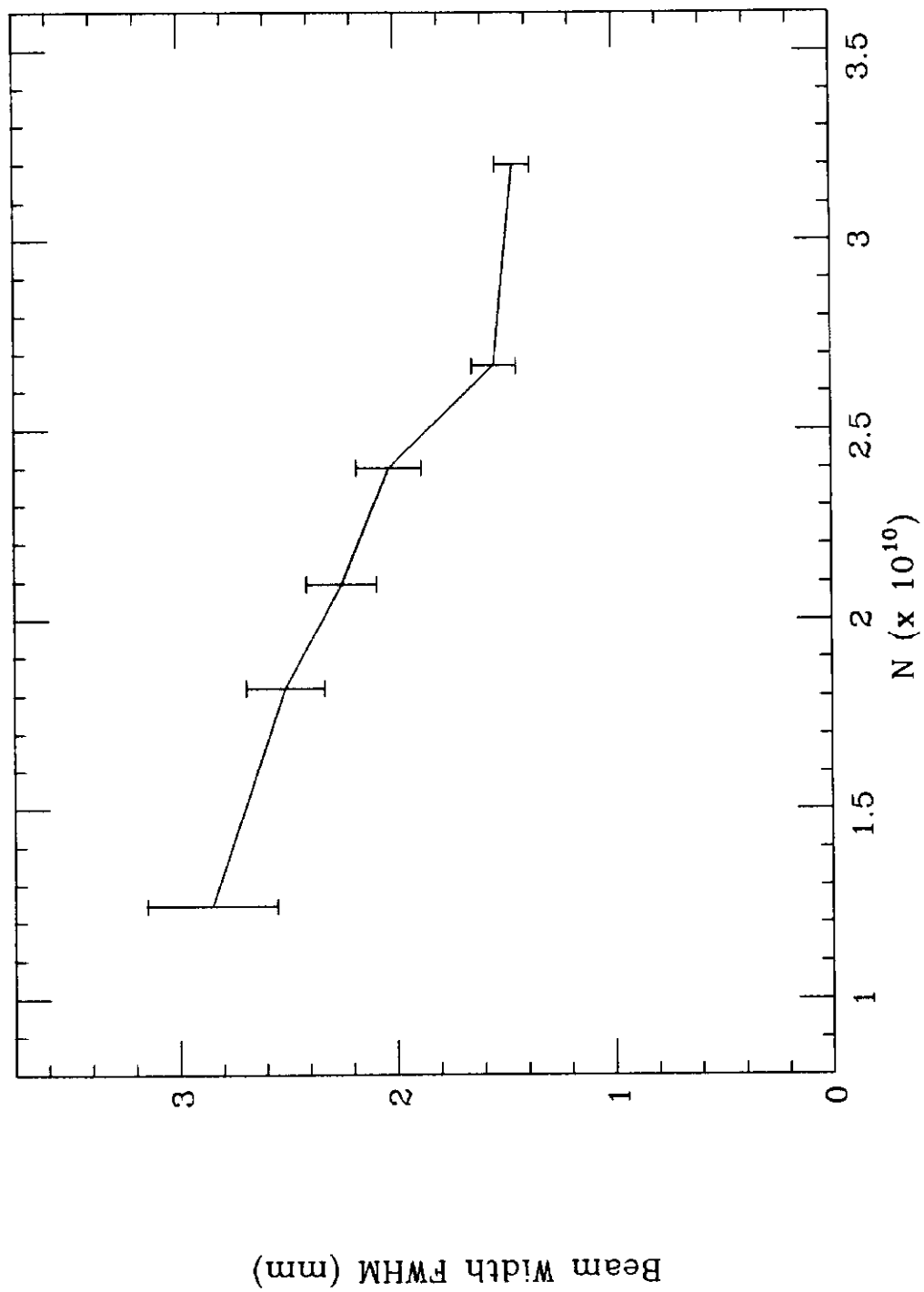


Figure 8